ACS OMEGA

http://pubs.acs.org/journal/acsodf

Mini-Review

Recent Advances and Challenges in Light Conversion Phosphor Materials for Third-Generation Quantum-Dot-Sensitized Photovoltaics

Ramkumar Sekar, Arrthi Ravitchandiran, and Subramania Angaiah*

Cite This: *ACS Omega* 2022, 7, 35351−35360

Read Online

ACCESS | Metrics & More | Article Recommendations | Supporting Information

ABSTRACT: Photovoltaic (PV) technologies have received tremendous attention for producing clean and renewable energy from the Sun. Third-generation quantum-dot-sensitized solar cells (QDSCs) present promising alternatives to conventional silicon solar cells due to their unique properties such as simplicity in fabrication, lower processing temperature, high flexibility, semi-transparent nature, and a theoretical conversion efficiency of up to 44%. However, the light-harvesting QD materials used in these SCs allow for the absorption of a small portion (from 300 to 800 nm) of the solar spectrum due to their narrow band gap. The nonabsorption of UV and near-infrared (NIR) light limits the power conversion efficiency (PCE) of these SCs. Hence, a PV technique that efficiently uses the entire solar spectrum becomes essential. The incorporation of light conversion phosphor materials (LCs) in QDSCs is a promising technology to absorb the whole part of the solar spectrum and enhance the PCE of these SCs. This review presents an overview of the advantages and limitations of QDSCs, different types of lanthanide-based light conversion phosphor materials, their synthesis and light conversion mechanism, and their influence on QDSCs.

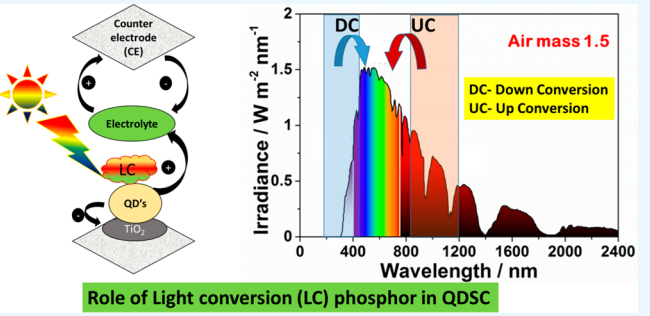

1. INTRODUCTION

Energy production from nonrenewable fossil fuels is facing huge problems because of their scarcity and environmental impact, which need to be resolved. Hence, transport and electricity markets around the world are moving toward alternative renewable energy sources to reduce pollution and generate electric power simultaneously. Solar energy, biomass, tides, hydro energy, and geothermal energy are renewable energy sources. Solar energy trumps all renewable energy sources because of its free availability, applicability for commercial and residential uses at a lower cost, and clean nature. Currently, the PV market is dominated by first-generation high-cost crystalline silicon (c-Si) panels and second-generation thin-film solar panels, which are made up of cadmium telluride (CdTe), gallium arsenide (GaAs), copper indium diselenide ($CuInSe_2$), copper indium gallium selenide ($CuInGaSe_2$, CIGS), and amorphous silicon (a-Si). Even though these kinds of solar cells show high efficiency, their manufacturing cost, scarcity, and toxic nature of the materials used are hurdles to large-scale production. Third-generation solar cells are suitable alternatives in PV industries. Dye-sensitized solar cells (DSSCs), quantum-dot-sensitized solar cells (QDSCs), organic solar cells (OSCs), and perovskite solar cells (PSCs) are known as third-generation solar cells. Among these, QDSCs are potential cost-effective candidates due to the easy availability of raw materials, simple fabrication process, portable nature, and excellent performance under diffused light conditions, making them promising candidates in PV industries.

Further, these SCs are solution-processed and can be fabricated on flexible substrates. Hence, these are potential devices to make wearable and flexible electronics for indoor applications. Apart from these merits, the lower efficiency of these devices is a hurdle to their commercialization. In general, light-absorbing materials in SCs absorb only a certain amount of energy from incident photons that match their energy gap. The incident photons with excess energy could be wasted as heat, and lower-energy photons simply pass through the devices without affecting their performance; hence, an energy conversion efficiency beyond the traditional Shockley and Queisser limit is impossible in single-junction PVs. This transmission loss of sub-band-gap photons could be manipulated using a multijunction device or incorporating light conversion materials in the device architecture. The construction of multijunction devices is challenged by their cost.

Received: June 15, 2022
Accepted: September 16, 2022
Published: September 30, 2022

https://doi.org/10.1021/acsomega.2c03736
ACS Omega 2022, 7, 35351−35360

Hence, using light conversion materials in QDSCs is a highly acceptable way to make efficient devices. Lanthanides are called light-converting materials and show application in different fields, including biomedical engineering, IR detection, biosensors, optical amplification, thermal sensing, photodetection, plasma panel devices, field emission display devices, light emitting diodes, color televisions, cathode ray oscilloscopes, cathode ray tubes, photoluminescent tubes, and photovoltaics. Lanthanides emit photons, having energy higher or lower than the absorbed photons through upconversion/downconversion (UC/DC) processes. These emitted photons are mostly available in the visible and near-infrared (NIR) region, where the light-harvesting materials of QDSCs absorb. So far, significant performance enhancements due to photon conversion technologies have not been reported in QDSCs, and a limited number of articles is available in this field. Hence, more efforts are required to design and develop high-efficiency phosphor materials that are energetically matched with QDs and suitable architectures to couple the light converters into QDSCs.

This review focuses on the enhancement of the PCE of QDSCs by using lanthanide-ion-doped phosphor materials. It begins with a brief description of the component materials, device structure, and working principle of QDSCs, followed by a detailed description of all the lanthanide ions, their energy levels with term symbols, UC and DC processes, and various synthesis methods. Then, publications dealing with lanthanide-doped light conversion materials and their role in enhancing the PCE of QDSCs are discussed. The operating principle of spectral converters in SCs is also discussed. Additionally, suggestions to improve the PCE and stability of QDSCs have also been included in the Conclusion and Prospects.

2. QDSCS

Quantum dots (QDs) are spherical nanomaterials with average diameters in the range of 2−10 nm. QDs have been extensively studied for PVs due to their size-dependent photoemission characteristics, quantum confinement effect, large extinction coefficients, high photostability, and solution processability. Further, QDs generate multiple charge carriers with a single photon. This phenomenon of QDs shows a theoretical efficiency of up to 44%, higher than the current Shockley−Queisser limit of 33%.[1] QDSCs consist of a wide-band gap mesoporous oxide film coated on a rigid glass substrate ($F:SnO_2$) as a photoanode, QDs as light-harvesting sensitizers, an electrolyte, and a counter electrode. Transition-metal oxides such as titanium dioxide (TiO_2), zinc oxide (ZnO), and tin dioxide (SnO_2) are the most intensely studied charge transport materials for QDSCs because of their superior chemical and thermal stability as well as their distinct electrical and optical properties. The redox couple between the photoelectrode and the counter electrode in QDSCs are used to regenerate the oxidized QDs. The most commonly used redox couple is the I^-/I_3^- liquid electrolyte. The counter electrode consists of a rigid glass substrate with an $F:SnO_2$ layer. Here, Pt or carbon material is deposited on top of the substrate. Widely used QDs in SCs are Ag_2S, Ag_2Se, CdS, CdSe, CdTe, ZnSe, ZnS, PbS, PbSe, $AgInS_2$, $AgInSe_2$, $CuInSe_2$, CdS_xSe_{1-x}, $CdSe_xTe_{1-x}$, etc. The size and chemical composition of the QD plays a major role in the emission wavelength and quantum yield. Several reports are available of core/shell QD systems such as CdSe/CdS, ZnTe/ZnSe, ZnSe/CdS, and CdSe/ZnSe. In these systems, shells with different thicknesses and compositions were grown on the core structure. By adjusting the thickness and composition of the shell structure, the emission wavelength has been tuned from the near-ultraviolet through the visible into the near-infrared region of the electromagnetic spectrum.

QDs can be introduced into the porous layer by *in situ* growth, directly from precursor solutions, or by adsorption of presynthesized QDs. Chemical bath deposition (CBD) and successive ionic layer adsorption and reaction (SILAR) are two widely used techniques for preparing the *in situ* growth of QDs. Here, QDs with the desired size, structure, etc. have been controlled by the growth conditions, such as the duration of deposition, precursor composition, and temperature of the solution. Currently, a PCE of 18.1% has been achieved in QDSCs. The PCE of QDSCs is far less than that of commercial Si PVs and the corresponding theoretical value (44%). Hence, to enhance the efficiency, several strategies such as increasing the concentration of QDs on the photoanode, reducing the recombination rate by introducing an interfacial layer, and introducing high-performance QDs, electrolytes, and counter electrodes have emerged. Technically, the performance of QDSCs can be directly related to their light absorption quality. However, these QDs absorb the solar spectrum only in the visible region. Thus, materials and methods need to be developed to enhance the absorption of QDSCs. When lanthanide light converters (LC) are combined with QDs, widening light harvesting from the UV to NIR region is possible.

3. LANTHANIDE-BASED PHOSPHOR MATERIALS

Lanthanides (Ln) are a group of 15 naturally occurring metallic elements in the periodic table. Their trivalent ions (Ln^{3+}) are highly stable. These 15 trivalent lanthanide ions (Ln^{3+}) are lanthanum (La^{3+}, $4f^0$), cerium (Ce^{3+}, $4f^1$), praseodymium (Pr^{3+}, $4f^2$), neodymium (Nd^{3+}, $4f^3$), promethium (Pm^{3+}, $4f^4$), samarium (Sm^{3+}, $4f^5$), europium (Eu^{3+}, $4f^6$), gadolinium (Gd^{3+}, $4f^7$), terbium (Tb^{3+}, $4f^8$), dysprosium (Dy^{3+}, $4f^9$), holmium (Ho^{3+}, $4f^{10}$), erbium (Er^{3+}, $4f^{11}$), thulium (Tm^{3+}, $4f^{12}$), ytterbium (Yb^{3+}, $4f^{13}$), and lutetium (Lu^{3+}, $4f^{14}$) (Table S1). La^{3+} has no f electrons, and Lu^{3+} has a filled f orbital. The remaining ions possess an incomplete 4f shell; hence, a large number of energy levels are possible due to the Coulomb interaction and the spin−orbit interaction between f electrons. These energy levels are denoted by the term symbol $^{2S+1}L_J$, according to the Russell−Saunders (L-S) notation. As per the selection rule, the f−f transitions are Laporte forbidden. However, when Ln^{3+} ions are incorporated into the host lattice, the surrounding crystal field developed by the host material destroys the spherical symmetry of its electronic structure. This somewhat relaxes the parity selection rule, and promoting f−f electron transitions. The process is called an induced electric dipole transition, giving rise to optical absorption and emission with reasonable intensities. The energy level diagrams of the trivalent lanthanide ions from Ce^{3+} to Yb^{3+} are shown in Figure S1.[2] As the f shell is shielded from the environment by the outer filled 5s and 5p orbitals, well-separated narrow lines occur rather than overlapped broad bands. These discrete emission lines with defined wavelengths are independent of the host materials' chemical composition and physical dimension. However, their intensities are highly determined by the surrounding environment. Further, the transfer of a 4f electron into a 5d subshell is possible in Ce^{3+}, Pr^{3+}, and Tb^{3+} RE ions. Compared to the f−f transition, this f−

https://doi.org/10.1021/acsomega.2c03736
ACS Omega 2022, 7, 35351−35360

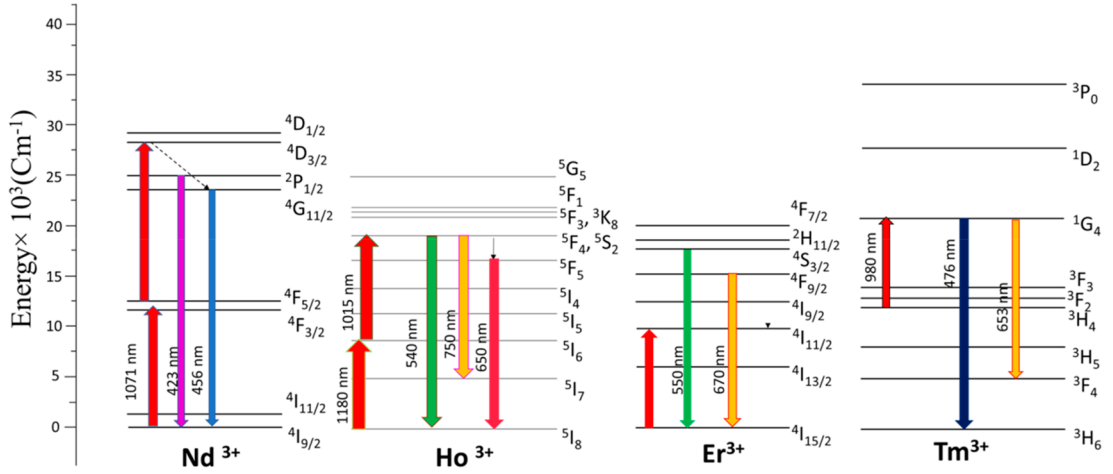

Figure 1. Energy level diagram and principal transitions of Nd^{3+}, Ho^{3+}, Er^{3+}, and Tm^{3+} upconverters.

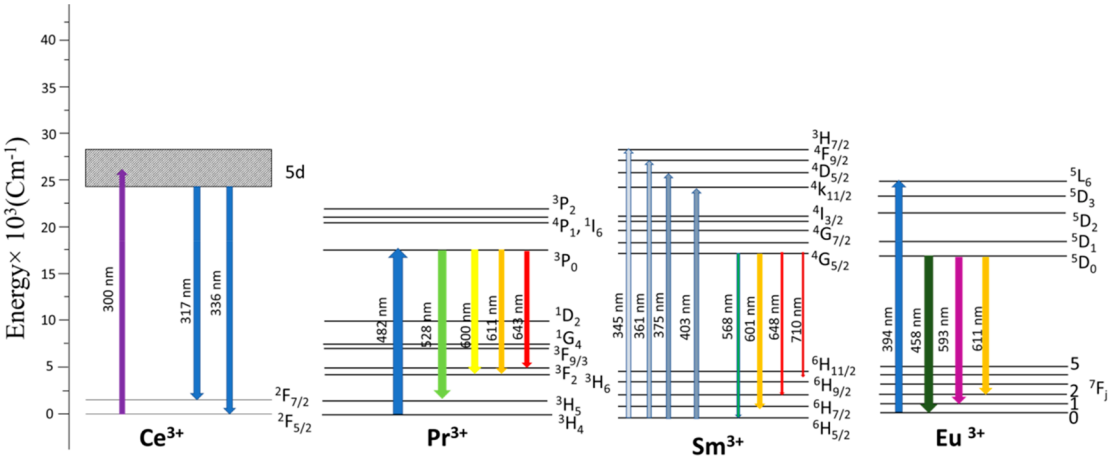

Figure 2. Energy level diagram and principal transitions of Ce^{3+}, Pr^{3+}, Sm^{3+}, and Eu^{3+} downconverters.

d transition gives a broad and high-energy spectrum. This transition is parity allowed, and 5d orbitals are external and interact directly with the host environment. Hence, two kinds of transitions are possible in RE ions: an f−f transition and a transfer of a 4f electron into a 5d subshell. These transitions between energy levels give a many-line spectrum in the visible and near-infrared (NIR) region. Due to these optical properties, trivalent lanthanide ions are proposed to be luminescent converters in PV devices. In the Ln series, the promethium (Pm^{3+}) ion cannot be used in PVs because of its radioactive nature.

4. LIGHT CONVERSION PHENOMENON

When a photon is passed through a lanthanide-based phosphor material, the energy of the emitted photon is either higher (anti-Stokes shift) or lower (Stokes shift) than the incident photon. In Stokes shift photoluminescence, absorbed higher-energy photons are emitted as lower-energy photons. On the other hand, in anti-Stokes photoluminescence, phosphors generate higher-energy photons than those used for the excitation. Based on this, several distinct optical processes, mainly downshifting (DF), downconversion (DC), and upconversion (UC), are possible in lanthanide ions due to their complex energy levels. A detailed explanation of this phenomenon associated with lanthanide ions is illustrated in the following sections.

4.1. Upconversion (UC). Ions absorb two low-energy sub-band-gap photons and are excited from the ground energy level to a higher energy level through an intermediate level while relaxing back to the ground state; they emit higher energy photons. This process was first reported by Auzel in 1966.[3] Generally, upconversion ions absorb two NIR photons and emit a single UV/visible photon. It has been reported that the conversion of NIR to visible light is comparatively easier than that of NIR to UV.

4.1.1. Upconversion of Ln^{3+} Ions. In the Ln^{3+} series ions Nd^{3+}, Ho^{3+}, Er^{3+}, and Tm^{3+} act as upconverters. However, these ions show several absorptions and emission lines; the mainly occurring principal transitions with their corresponding energy states are depicted as follows[4] (Figure 1).

Nd^{3+} absorbs NIR photons and is excited from the ground energy level, $^4I_{9/2}$. From this, it emits light in the visible region.

Ho^{3+} absorbs NIR photons and is excited from the ground energy level of $^5I_8$ to the degenerate higher energy level of $^5S_2$ and $^5F_4$ through the intermediate energy level $^5I_6$. Relaxation photoemission occur in the visible region typically at 540, 650, and 750 nm for the electronic transitions $^5F_4$, $^5S_2 \rightarrow {}^5I_8$, $^5F_5 \rightarrow {}^5I_8$, and $^5F_4$, $^5S_2 \rightarrow {}^5I_7$, respectively.

Er^{3+} absorbs NIR photons and is excited to the higher energy level of $^4F_{7/2}$ from the ground energy level $^4I_{15/2}$ through the intermediate energy level $^4I_{11/2}$. Relaxation

https://doi.org/10.1021/acsomega.2c03736
ACS Omega 2022, 7, 35351−35360

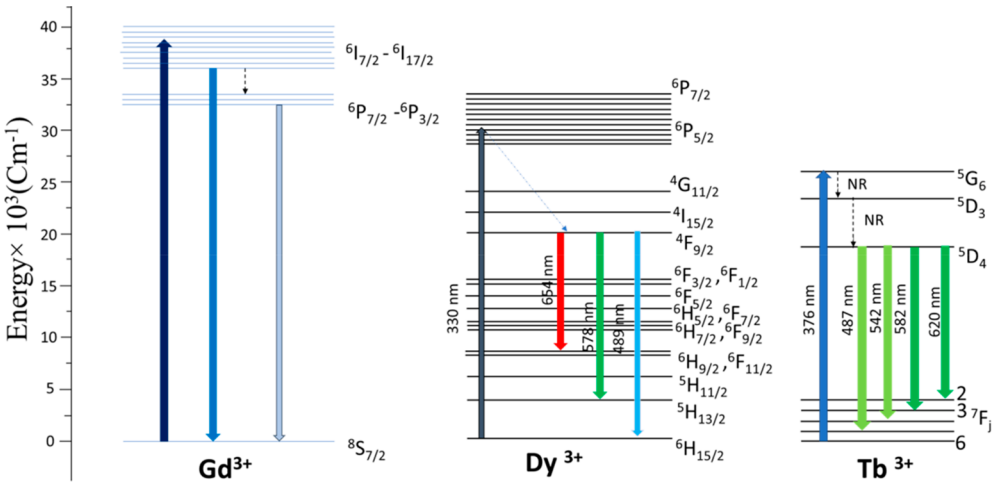

Figure 3. Energy level diagram and principal transitions of Gd^{3+}, Dy^{3+}, and Tb^{3+} downconverters.

typically gives strong UC emission between 550 and 670 nm, based on the transitions $^4S_{3/2}$, $^4F_{9/2} \rightarrow {}^4I_{15/2}$.

Tm^{3+} ions absorb NIR light at 980 nm and are excited to the higher energy $^1G_4$ state. They then emit light in the visible region for the electronic transitions $^1G_4 \rightarrow {}^3H_6$ (476 nm) and $^1G_4 \rightarrow {}^3F_4$ (653 nm).

4.2. Downconversion (DC). In a DC process, ions absorb a high-energy photon and are excited from the ground energy level to a higher-energy level. Returning to the ground state causes relaxation to an intermediate energy level. The ion emits either one (downshifting process) or two (downconversion process) lower-energy photons. Since two photons are emitted from a single photon, a quantum efficiency (QE) of up to 200% is possible in the DC process. This phenomenon was first proposed by Dexter in the 1957.[5] Trupke et al. in 2002 theoretically predicted that adding an ideal DC phosphor material to a silicon solar cell enhances its PCE from 30.9% to 38.6%.[6]

4.2.1. Downconversion of Ln^{3+} Ions. Ce^{3+}, Pr^{3+}, Sm^{3+}, Eu^{3+}, Gd^{3+}, Tb^{3+}, and Dy^{3+} play roles as downconverters. The principal transitions with their corresponding energy states of these ions are depicted as follows[7] (Figures 2 and 3).

Ce^{3+} ($4f^1$) contains only two ^2F states ($^2F_{5/2}$ and $^2F_{7/2}$). It absorbs UV light at around 300 nm corresponding to the electronic transition of 4f → 5d states. A nonradiative relaxation process to the lower 5d state occurs and then emits light at 317 nm (5d → $^2F_{7/2}$) and 336 nm (5d → $^2F_{5/2}$).

Pr^{3+} ions absorb photons at a wavelength of 482 nm and are excited from the ground state energy level $^3H_4$ to the higher-energy levels $^3P_0$, $^3P_1$, and $^3P_2$. The photoluminescence emission occurs in the NIR range due to the electronic transition $^3P_0$ to the lower energy levels.

Sm^{3+} absorbs near-ultraviolet radiation around 375−405 nm and emits at 567, 600, 647, and 710 nm due to transitions from the excited state $^4G_{5/2}$ to ^6H_j (j = 5/2, 7/2, 9/2, 11/2), respectively.

Eu^{3+} absorbs UV light with the wavelength range of 230−320 nm and emits at 394, 458, 593, and 611 nm, corresponding to the electron transitions $^5L_6 \rightarrow {}^7F_0$, $^5D_2 \rightarrow {}^7F_0$, $^5D_0 \rightarrow {}^7F_2$, and $^5D_0 \rightarrow {}^7F_1$, respectively.

Gd^{3+} absorbs UV light at around 280 nm and excites higher energy levels to ^6I_j (j = 7/2 to 17/2). It then emits sharp lines between 272 and 278 nm for the electronic transitions $^6I_{17/2}$, $^6I_{7/2} \rightarrow {}^8S_{7/2}$ and emits lines between 300 and 311 nm due to the transitions ^6P_j (j = 3/2, 5/2, 7/2) → $^8S_{7/2}$.

Tb^{3+} is excited from the ground state $^7F_6$ to higher-energy levels by absorbing UV light at 380 nm. It emits visible light in the region at 490, 545, 590, and 624 nm due to the electronic transitions $^5D_4 \rightarrow {}^7F_j$ (j = 6, 5, 4, 3).

Dy^{3+} absorbs UV−vis light from 330 to 460 nm, is excited to the $^6P_{7/2}$ level, and then relaxes nonradiatively to the $^4F_{9/2}$ level. It then emits light in the visible region due to the electronic transitions $^4F_{9/2} \rightarrow {}^6H_{15/2}$ (489 nm), $^4F_{9/2} \rightarrow {}^6H_{13/2}$ (578 nm), and $^4F_{9/2} \rightarrow {}^6H_{9/2}$ (654 nm).

4.3. Sensitizers. Yb^{3+} ions do not have the conversion ability like other ions. Yb^{3+} absorbs NIR photons at 980 nm and responds to the electron transition $^2F_{5/2} \rightarrow {}^2F_{7/2}$. It acts as a sensitizer and transfers the energy to other Ln metals such as Er^{3+}, Ho^{3+}, and Tm^{3+}. It also acts as a bridge and conducts energy between the donor (Nd^{3+}) ion and acceptor ions such as Er^{3+}, Tm^{3+}, Ho^{3+}, Pr^{3+}, and Tb^{3+}.[8] In some cases, the Nd^{3+} ion has also been proposed as a sensitizer. It has absorption at 808 nm and transfers this energy to the Yb^{3+} ion.[9]

5. SYNTHESIS OF LIGHT CONVERSION PHOSPHORS

In general, rare-earth (RE)-ion-doped UC/DC phosphors are prepared by adding a small concentration of either one or more than one RE lanthanide ions, called activator ions, into the inert host material, normally an oxide, fluoride, silicate, phosphate, nitride, sulfide, or oxysulfide (Figure 4). The host determines the crystal structure, whereas the activator ions convert the light.

The choice of the host matrix mainly depends on the ionic radius and its close band alignment levels to the activator ion. The host cation gets suitably replaced in the chosen matrix with the RE^{3+} ion. Hence, the ionic radius of the host cation must be similar to that of the dopant activator ion. Further, an ideal host material should have (i) low lattice phonon energies

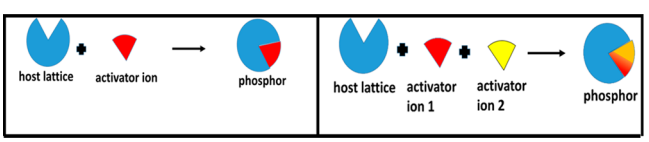

Figure 4. Schematic illustration of the preparation of phosphor materials with single and multiple activator ions.

https://doi.org/10.1021/acsomega.2c03736
ACS Omega 2022, 7, 35351−35360

to suppress nonradiative losses (this is highly related to the lattice vibrations of atoms in the host matrix) and (ii) a highly crystalline structure with few lattice defects and impurities. Suppose the host materials have poor crystallinity, lattice defects, and impurities. In that case, the energy absorbed by a RE^{3+} ion can dissipate to the defect of the host lattice and then recombine nonradiatively. This affects the light conversion performances of the phosphor material. To maintain the crystalline phase of the host, the dopant concentration should be strictly controlled.

As we have seen, the light conversion property, quantum efficiency, emission wavelength, and thermal stability of the phosphor materials are highly related to their morphology, size, purity, crystalline structure, and compositions. Hence, these properties are very significant to getting a better solar cell performance. For example, the hexagonal β-phase of $NaYF_4$ exhibits higher UC efficiency than its cubic α-phase. As has been noted in the literature, the conversion of the α-phase to β-phase can be controlled by the temperature of the reaction process.[10] Chen et al. prepared CeO_2:Eu^{3+} DC phosphors with different morphologies, crystalline sizes, and emission properties by varying the hydrothermal treatment times (2, 4, 8, 12, 16, and 20 h). They proposed that DC phosphors with an octahedral, mirrorlike structure and a size of 70 nm obtained at 12 h reaction time exhibited excellent DC luminescence, light scattering properties, and improved solar device efficiency by 35% relative to the reference undoped devices.[11] Saleh et al. prepared the deep red-emitting Sm^{3+}- and Eu^{3+}-doped calcium scandate ($CaSc_2O_4$ (CSO)) phosphors by a solid-state route. The light absorption capability, emission property, and thermal stability of the CSO have been controlled by changing the concentration of Eu^{3+} dopant. The solar devices coated with a CSO layer displayed a high PCE (15.96%) in comparison with those of the control devices.[12] $NaYF_4$:Yb/Er exhibits 2 times stronger UC luminescence efficiency than that of $NaLaF_4$:Yb/Er due to the smaller cation size of the host. The smaller yttrium cation strengthens the crystal field around the dopant ions and leads to enhanced UC efficiency.[13] Fine-tuning of the upconversion emission wavelength and emission intensity might also be possible by precisely controlling different combinations of lanthanide dopants and dopant concentration within a single host source. Huy et al. controlled the upconversion emission colors of Y_2SiO_5:Yb^{3+},Er^{3+} nanoparticles by the precise control of the concentration of Yb^{3+} ions. They proposed that the red to green (R/G) ratio of the phosphor increases with increasing Yb^{3+} concentration.[14] The synthesis method involved has been shown to strongly determine the key optical properties of the phosphor. Hence, developing a new methodology to synthesize the phosphor material with desirable optical properties has gained wide attention in this PV area. Several synthesis methods, such as sol−gel, hydrothermal, and high-temperature solid-state reactions, thermal decomposition, etc., are available in the literature (Figure 5). These preparation methods differ in their processing time, degree of complexity, equipment used, cost, and many others. Simple, environmentally friendly, and low-cost methods are acceptable. However, the preference is based on the desired properties of the prepared phosphors.

The sol−gel method offers an easy way to synthesize the phosphors at a low cost and ambient processing temperature. In a sol−gel method, precursors of rare-earth ions such as oxides, acetates, chlorides, and nitrates are mixed with host precursors such as fluorides or oxides ($BaTiO_3$, YVO_4, Y_2O_3, $NaYF_4$, GdF_3, and TiO_2) in an aqueous or alcoholic medium. Hydrolysis reagents, surfactants, and co-surfactants can also be added to the solution to initialize the hydrolysis/condensation process. While this method is considered to be cost-effective, the lack of regulation of the particle size and substantial aggregation limits this process. This could be nullified by a hydrothermal process.

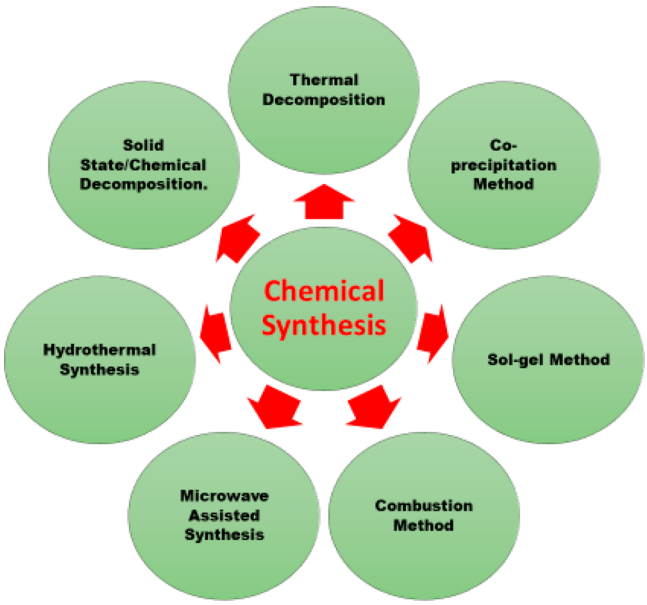

Figure 5. Synthesis of lanthanide-doped phosphor materials.

The precursor solutions have been mixed thoroughly and placed in a Teflon-lined stainless-steel autoclave in a hydrothermal method. The autoclave is sealed and heated to a critical temperature above the solvent's boiling point. Here, the reaction occurs due to the high pressure and temperature created. The reactor's opacity is the primary drawback, and monitoring the reaction progress is impossible. In both sol−gel and hydrothermal processes, the formation/growth of phosphor materials is determined by the experimental parameters, such as precursor concentration, catalyst, surfactants, pH of the solution, reaction temperature, and time.

Thermal decomposition is another approach for preparing phosphors. In this method, decomposition of the reactants is carried out in high-boiling organic solvents such as octadecene (ODE), oleic acid (OA), and oleylamine (OM) under inert reaction conditions. Nanophosphor materials such as Er^{3+}-/Yb^{3+}-doped $NaYF_4$ and Ho^{3+}-/Yb^{3+}-doped Gd_2O_3 were prepared by this method. Synthesizing a few nanometer-sized phosphors is possible in this method. However, the use of hazardous solvents and toxic byproducts in these processes poses a potential threat to the environment and severely compromises the biocompatibility of the phosphors in industrial PVs.

The coprecipitation method is a widely accepted technique because of its industrial perspective. In a typical process, high-quality phosphors have been synthesized by adding a precipitating agent such as a base to a solution containing inorganic rare-earth salts and host precursors. The crystallite size and morphology of the prepared phosphor material can be controlled by varying temperatures, solvents, and precipitating agents. The required continuous washing, drying, and calcination to achieve a pure phase of the phosphor are the major disadvantages of this method.

https://doi.org/10.1021/acsomega.2c03736
ACS Omega 2022, 7, 35351−35360

Solid-state synthesis is a well-known and traditional method for synthesizing RE-doped UC/DC phosphors. To incorporate the RE ions into the host, raw solid precursors in the required quantity are thoroughly powdered, heated above their melting temperatures, and then allowed to cool. The cooling rate should be as slow as possible to obtain a single crystal with good crystallinity. The advantages of this method are obtaining homogeneous mixing of metal ions at the molecular level and obtaining ultrasmall particles with a high packing density.

The combustion technique is another unique method of synthesizing phosphor materials. To initiate combustion, a fuel and oxidizer are required. RE metal nitrates are used as oxidizers, and hydrazine-based compounds, urea, or glycine are employed as fuels. As this reaction occurs at a higher temperature, further calculations and repeated heating of the phosphors are not required in this process.

Microwave technology is a fast and energy-efficient synthesis technique for phosphors. In a conventional oil bath heating method, phosphors with different morphologies and sizes are possible due to the inhomogeneous temperature profiles within the reaction flask. Microwave reactors can produce rapid and uniform heating for the sample solution. This quick transfer of energy to the precursors causes their rapid breakdown, resulting in extremely supersaturated solutions where nucleation and growth can occur to form the required phosphor. However, the microwave synthesis reactor is expensive, and scaled-up production has not yet been reached.

6. PHOSPHORS IN QDSCS

The introduction of UC/DC phosphors in QDSCs facilitates improving the efficiency and stability of solar cells. As DC phosphors split a high-energy photon into two low-energy photons, a quantum efficiency (QE) of up to 200% is possible in the DC process. UV-induced thermal degradation of electrolyte components is possible in QDSCs. The incorporation of the DC materials into the SCs can not only increase the PCE via conversion luminescence and light scattering but also improve the lifetime of the SC by the absorption of UV light. However, the large-sized particles in photoanode films may form agglomerates and lower the device efficiency by increasing the device resistance. The basic concepts and development of QDSCs using lanthanide ions as light conversion materials reported by researchers worldwide are discussed in the upcoming section. The energy transfer from LCs to QDs has been studied by Li et al. for effective photocatalysis.[15] Mercaptoethanol-functionalized upconversion $NaYF_4$:Yb,Tm microrods were prepared and combined with CdS QDs. To examine the energy transfer process from $NaYF_4$:Yb,Tm to CdS QDs, the upconversion emission spectra of the composite were recorded upon 976 nm NIR excitation (Figure 6a). The intensity of UV and blue emission peaks of LCs is significantly reduced after the combination with CdS, indicating a significant energy transfer. The following mechanism was proposed for energy transfer: Yb absorbs the NIR photons and transfers the energy to the Tm ions. On relaxation, Tm produces UV emissions at 350−361 nm, blue emissions at 450−470 nm, and red emissions at 645 nm. These emitted photons excited the CdS QDs, as the energy gap of CdS is about 2.5 eV, which is lower than the emitted blue and UV photon energy (Figure 6b).

This energy transfer mechanism has been reported for several LC materials involved in QDSCs. Strontium aluminate doped with Eu and Dy ions has been investigated as an

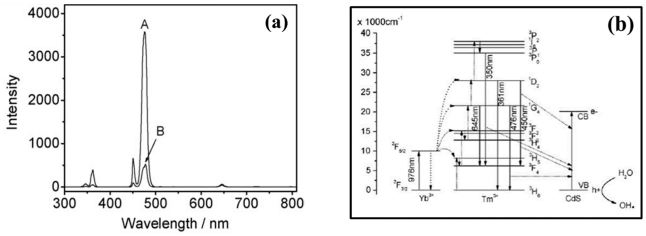

Figure 6. (a) Upconversion emission spectra of (A) $NaYF_4$:Yb,Tm and (B) $NaYF_4$:Yb,Tm/CdS. (b) Schematic illustration of the energy transfer mechanism from $NaYF_4$:Yb,Tm to CdS upon 976 nm NIR irradiation. Reproduced with permission from ref 15. Copyright 2010 Elsevier BV.

efficient downconverting phosphor material for PVs because it emits photons at a wavelength of around 500 nm, has high quantum efficiency, and good stability. The $SrAl_2O_4$:Eu,Dy phosphor was introduced into the TiO_2 photoanode by screen printing to fabricate QDSCs. It increases the photovoltaic performances of the cells by 26.5% in comparison to a cell without the phosphor material. The $SrAl_2O_4$:Eu,Dy used acts not only as a downconverting layer but also as a scattering layer.[16] Later, it was realized that the $SrAl_2O_4$:Eu,Dy emission wavelength of 512 nm could not be effectively absorbed by CdS QDs, as its E_g value is 2.4 eV. To rectify this, CdS was replaced with narrower-band-gap CdSe QDs (1.7 eV). QDSCs were fabricated using CdSe QDs consisting of long-afterglow $SrAl_2O_4$:Eu,Dy phosphors on top of the TiO_2 layer. The cell with $SrAl_2O_4$:Eu,Dy shows a conversion efficiency of 1.22%, 48% more than that of the bare cell (0.82%).[17] In another approach, the $SrAl_2O_4$:Eu,Dy phosphor was replaced with $Sr_4Al_{14}O_{25}$:Eu, Dy. This phosphor emits light at 490 nm and matches the band gap of CdS QDs. $Sr_4Al_{14}O_{25}$:Eu,Dy enhances the performances of the cells by up to 38%. The light scattering and downconverting capability of a P25/$Sr_4Al_{14}O_{25}$:Eu,Dy electrode was analyzed through UV−vis diffuse reflection (Figure 7a) and PL excitation and emission (Figure 7b) spectroscopy, respectively. It was observed that the P25/$Sr_4Al_{14}O_{25}$:Eu,Dy electrode has a higher light reflectance than the bare P25 electrode and emits a broad emission spectrum with a peak at 490 nm, which falls well in the absorption range of the CdS QDs.[18] Notably, the phosphors $SrAl_2O_4$:Eu,Dy and $Sr_4Al_{14}O_{25}$:Eu,Dy emit light to drive the QDSCs even when the light source is turned off after illumination. Hence, they are named long-persistence phosphors (LPPs).

On this basis, Deng et al. introduced a long-persistence phosphor (LPP) layer into the CdS/CdSe QDSCs via a simple doctor blade method. The LPP layer can simultaneously improve the light-harvesting and photo charge transfer in CdS/CdSe QDSCs. As a result, the PCE can reach up to 5.07%, which is about 24% higher than the conventional CdS/CdSe QDSCs without the LPP layer. The fabricated solar cells even worked in the dark for a while due to the long-lasting fluorescence of the LPP layer. UV-induced thermal degradation of electrolyte components is possible in QDSCs. Wang et al. synthesized an upconverting Yb^{3+}-/Er^{3+}-/Tm^{3+}-codoped $NaYF_4$ (Ln-$NaYF_4$) phosphor material through a hydrothermal method and used it as a photoanode for CdS-/CdSe-based QDSCs (Figure 8a). Ln-$NaYF_4$ converted NIR light to visible light due to the upconversion process, and this emitted light was absorbed by the QDs. This indirect usage of the NIR light enhanced the PCE of SCs. In this way, the added upconverters

https://doi.org/10.1021/acsomega.2c03736
ACS Omega 2022, 7, 35351−35360

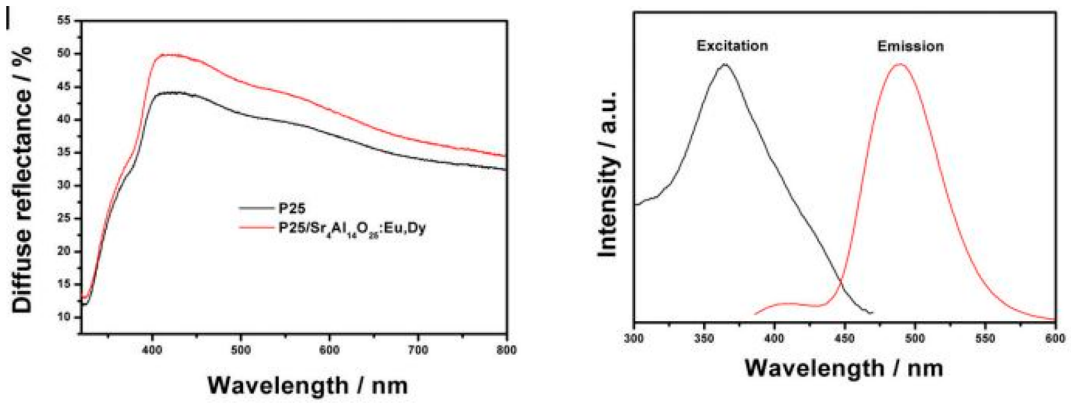

Figure 7. (a) UV−vis diffuse reflectance spectra of the P25 and P25/$Sr_4Al_{14}O_{25}$:Eu,Dy electrodes, (b) PL excitation and emission spectra of $Sr_4Al_{14}O_{25}$:Eu,Dy (λ_{ex} = 365 nm, λ_{em} = 490 nm). Reproduced with permission from ref 18. Copyright 2014 The Royal Society of Chemistry.

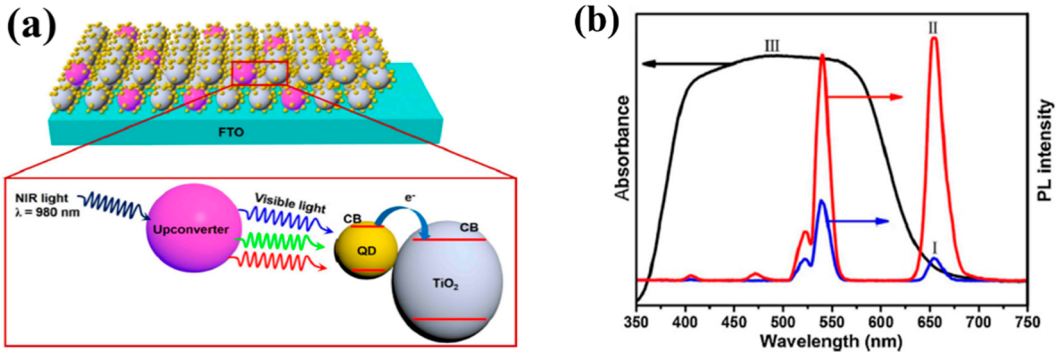

Figure 8. (a) Schematic illustration of the upconverter-based electrode for QDSCs. (b) Upconversion emission spectra of the synthesized Ln-$NaYF_4$ (I) and the sample annealed at 700 °C (II) under laser excitation with a wavelength of 980 nm and a UV−vis absorption spectrum of the QDs anchored on the electrode (III). Reproduced with permission from ref 19. Copyright 2014 Elsevier Ltd.

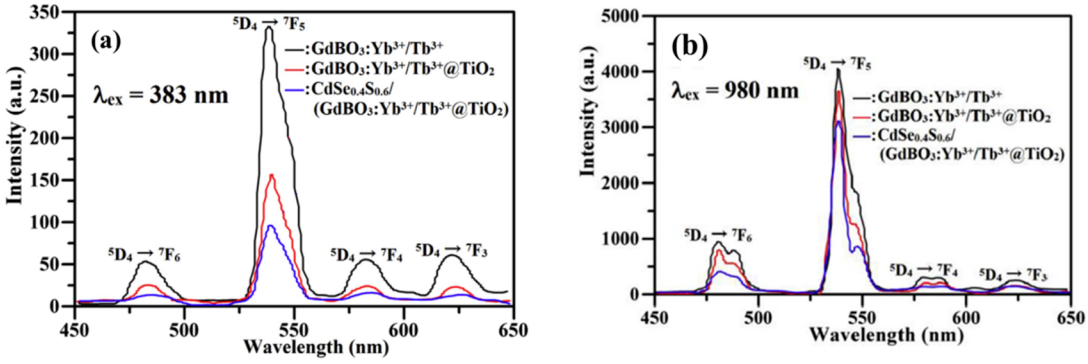

Figure 9. Photoluminescence spectra of $GdBO_3$:Yb^{3+}/Tb^{3+}, $GdBO_3$:Yb^{3+}/Tb^{3+}@TiO_2, and $CdSe_{0.4}S_{0.6}$/$GdBO_3$:Yb^{3+}/Tb^{3+}@TiO_2 nanoparticles with a 1.0% addition of of $GdBO_3$:Yb^{3+}/Tb^{3+}: (a) excited at 383 nm; (b) excited at 980 nm. Reproduced with permission from ref 23. Copyright 2018 Elsevier BV.

enhanced the PCE from 3.43% to 4.13%. Furthermore, to eliminate the defects in Ln-$NaYF_4$, it was annealed at 700 °C. The optical properties of the prepared samples are shown in Figure 8b. The annealed sample shows stronger upconversion fluorescence intensity along with two new emission peaks at around 400 and 475 nm. These new peaks are assigned to the electronic transitions $^2P_{3/2} \rightarrow {}^4I_{13/2}$ of Er and $^1G_4 \rightarrow {}^3H_6$ of Tm, respectively. This optical enhancement is due to the pretreatment annealing process that eliminates the surface citrate groups in the crystals from the hydrothermal synthesis environment and produces a defect-free structure. The annealing-induced enhancement of the upconversion emission results in an obvious improvement in the PCE (4.37%).[19]

Ramachari et al. introduced the Yb^{3+}-Er^{3+}:ZrO_2 passivation layer in CdS-based QDSCs and effectively increased the PCE to 55%.[20] The Yb^{3+}-Er^{3+}:ZrO_2 layer is prepared by a facile coprecipitation method at low temperature followed by a high-temperature sintering treatment. The prepared Yb^{3+}-Er^{3+}:ZrO_2 layer was deposited on a TiO_2/CdS/ZnS photoanode by SILAR technique.

Metal−organic frameworks (MOFs) are hybrid materials that combine organic linkers with inorganic elements. They have received considerable attention in PVs due to their

https://doi.org/10.1021/acsomega.2c03736
ACS Omega 2022, 7, 35351−35360

fascinating chemical and physical properties, tunability, and extraordinary porosity. Kaur et al. prepared a CdTe/Eu-MOF nanocomposite using europium nitrate, 1,3,5-tris(4-carboxyphenyl) benzene, and cysteamine-capped CdTe QDs and achieved an 80% improvement in the PCE compared with bare CdTe QDs.[21] Meanwhile, binary/ternary lanthanum ion doped phosphors, i.e. Gd^{3+}-Eu^{3+}, Gd^{3+}-Tb^{3+}, Tb^{3+}-Yb^{3+}, Gd^{3+}-Er^{3+}-Tb^{3+}, etc., have also gained increasing attention for SCs. $GdBO_3$:Yb^{3+}/Tb^{3+} is one of the dual-ion-containing phosphor materials and has shown potential application in the energy field.[22] The presence of dual ions such as Tb^{3+}-Yb^{3+} in the phosphor is one of the promising combination systems, since the Tb^{3+} transition is located at 485 nm and the Yb^{3+} transition is located at 980 nm. Hence, combining these elements will absorb UV and NIR light and emit visible light ranging from 450 to 650 nm. Based on the above considerations, Fang et al. recently reported the application of bidirectional (up and down) $GdBO_3$:Yb^{3+}/Tb^{3+} luminescence materials in $CdSe_{0.4}S_{0.6}$ QDSCs. $GdBO_3$:Yb^{3+}/Tb^{3+} has been prepared by a sol−gel method and added to a tetrabutyl titanate solution to form $GdBO_3$:Yb^{3+}/Tb^{3+}@TiO_2 nanoparticles.[23]

The photoluminescence spectra have confirmed the light emission properties of the $GdBO_3$:Yb^{3+}/Tb^{3+}phosphor. Figure 9a,b shows the photoluminescence spectra of $GdBO_3$:Yb^{3+}/Tb^{3+}, $GdBO_3$:Yb^{3+}/Tb^{3+}@TiO_2, and $CdSe_{0.4}S_{0.6}$/$GdBO_3$:Yb^{3+}/Tb^{3+}@TiO_2 nanoparticles excited at 383 nm and excited at 980 nm, respectively. The decrease in the emission intensities may be caused by the $CdSe_{0.4}S_{0.6}$QDs, which have strong absorption in the visible light range. The bidirectional (up- and down-) conversion luminescence processes of the $GdBO_3$:Yb^{3+}/Tb^{3+}phosphor are depicted through the energy level diagram as shown in Figure 10. For

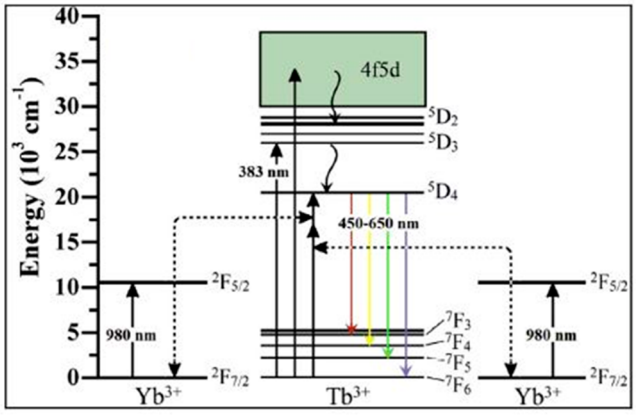

Figure 10. Energy level diagram and bidirectional (up- and down-)conversion luminescence processes of the $GdBO_3$:Yb^{3+}/Tb^{3+} phosphor. Reproduced with permission from ref 23. Copyright 2018 Elsevier BV.

each Tb^{3+} ion excitation, two Yb^{3+} ions are required. Yb^{3+}ions absorbed NIR photons at around 980 nm and transferred the energy to the Tb^{3+} ion for its excitation from the $^7F_6$ level to the $^5D_4$ energy level. At the same time, the Tb^{3+} ion itself absorbed the UV light at a wavelength of around 383 nm and was excited to $^5D_3$ energy level. After that, a nonradiative relaxation from the $^5D_3$ to $^5D_4$ energy level happens. Then, the exciting Tb^{3+} ion undergoes a radiative transition into lower energy levels (^7F_J, J = 3, 4, 5, 6), resulting in the emission of visible light (450−650 nm).

A transparent conducting oxide (TCO) substrate is one of the important components in PVs as it (i) acts as a backbone scaffold for the construction of devices, (ii) permits incident solar light to enter the cells, and (iii) conducts charges from the cell to the external circuit. A superior transmission of light in the visible and near-infrared regions, high electrical conductivity, and high thermal and chemical stability are the important criteria for TCOs. The most common TCO substrate in SCs is F-doped tin oxide (FTO) and indium tin oxide (ITO). A downconverting ITO glass substrate was used to further enhance the light absorption in the PbS/CdS-based QDSCs. The downconverting glass substrate was prepared by melt quenching using Er_2O_3, and the ITO film was deposited onto the doped phosphate substrate by magnetron sputtering. The fabricated device achieved a PCE of 8.6%.[24]

In general, lanthanide-doped phosphors display multipeak emission profiles, as lanthanide ions have more than one metastable excited state. Several attempts have been made to obtain a single emission band with high chromatic purity.[3] Wang et al. replaced the commonly used $NaYF_4$ host lattice with $KMnF_3$ and prepared the three phosphor nanocrystals $KMnF_3$:Yb/Er, $KMnF_3$:Yb/Ho, and $KMnF_3$:Yb/Tm.[25] A room-temperature photoemission spectrum indicated the emission properties of the prepared $KMnF_3$-based nanocrystals under the excitation of a 980 nm CW diode laser at a power density of 10 W cm^2. The PL emission with the corresponding energy transfer mechanism and luminescent photos of the colloidal solutions in cyclohexane are depicted in Figure 11. The Yb^{3+} ion absorbs the NIR photon at a wavelength of 980 nm and is excited from the ground energy level, $^2F_{7/2}$, to a higher energy level, $^2F_{5/2}$. Then it drops back to the ground state with simultaneous energy transfer to the adjacent ions (Er^{3+}, Ho^{3+}, and Tm^{3+}). Er^{3+}, Ho^{3+}, and Tm^{3+} ions normally emit these photons in the visible region. However, in combination with Mn^{2+} ions, nonradiative energy transfer from the $^2H_{9/2}$ and $^4S_{3/2}$ levels of Er^{3+}, $^5F_3$ and $^5F_4$ levels of Ho^{3+}, and $^1D_2$ and $^1G_4$ levels of Tm^{3+} to the $^4T_1$ level of Mn^{2+}, followed by back-energy transfer to the $^4F_{9/2}$ level of Er^{3+}, $^5F_5$ level of Ho^{3+}, and $^3F_2$ level of Tm^{3+} respectively occur. This produces a single band in the visible region. These observations proposed that the Mn^{2+} ion is an optimum codopant for the UC phosphors containing the Yb^{3+}/Er^{3+}, Yb^{3+}/Ho^{3+}, and Yb^{3+}/Tm^{3+} ions to obtain a highly intense single emission peak.

Based on this phenomenon, Sun et al. prepared Mn^{2+}, Yb^{3+}, Er^{3+} tridoped $NaYF_4$UC phosphors and doped them into TiO_2 photoanodes for fabricating CdS/CdSe based QDSCs.[25] Mn^{2+} ions enhanced the red emission of Er^{3+} ions and thus red-shifted the absorption of QD photoanodes. The light−electric conversion properties of QDSCs dependent on the different doping contents of UCNPs were systematically investigated. A maximum conversion efficiency of 4.75%, with an improvement of 42.6% compared to the UCNPs-free TiO_2 photoanode (3.33%), was achieved at the optimized composition of 8 wt % UCNPs/TiO_2.

7. CONCLUSION AND PROSPECTS

QDSC is a low-cost and effective green energy technology in PV industries. However, it demands novel and efficient technology support for practical commercialization. Currently, the absorption of QDs is comparatively inferior to that of other

https://doi.org/10.1021/acsomega.2c03736
ACS Omega 2022, 7, 35351−35360

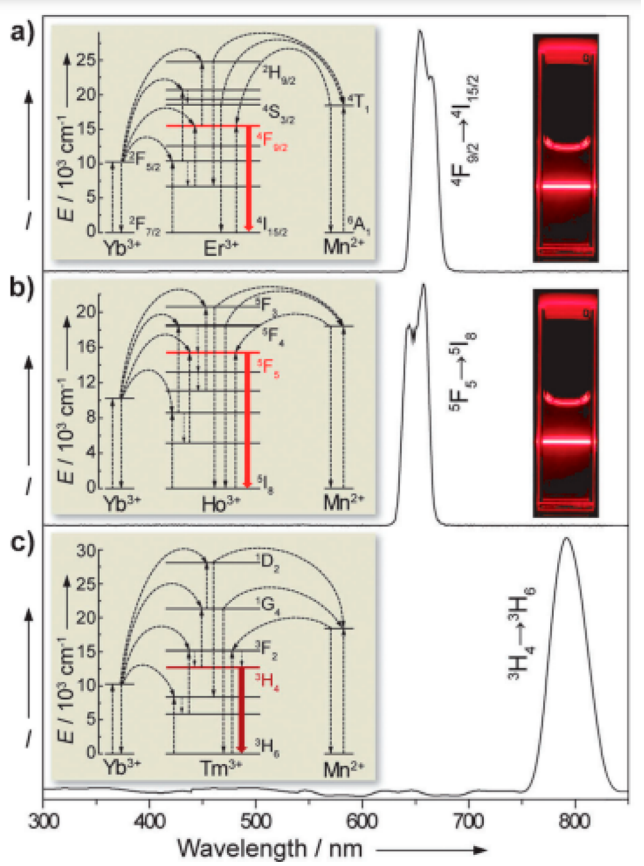

Figure 11. Room-temperature UC emission spectra of solutions containing (a) $KMnF_3$:Yb/Er (18:2 mol %), (b) $KMnF_3$:Yb/Ho (18:2 mol %), and (c) $KMnF_3$:Yb/Tm (18:2 mol %) nanocrystals in cyclohexane (insets: proposed energy transfer mechanisms and corresponding luminescent photos of the colloidal solutions). Reproduced with permission from ref 25. Copyright 2011 Wiley-VCH.

materials. Many efforts have been made to improve the PCEs of QDSCs by enhancing the optical absorption of QDs. Incorporating light conversion phosphor materials in the QDSC device structure is a scientifically accepted way to rectify this problem. Trivalent lanthanide ions having the electronic configuration $[Xe]4f^n$ (n = 0−14) are suitable materials for light conversion. Each of the n electrons is associated with one of the seven 4f orbitals. Therefore, the arrangement of electrons within this configuration is substantially diverse. Hence, a large number of energy levels are possible due to the Coulomb interaction and the spin−orbit interaction between f electrons. However, the electronic transition between these energy levels is symmetrically forbidden. The introduction of Ln^{3+} ions into the host lattice breaks the symmetry and allows the electron transition. Hence, Ln^{3+} absorbs and emits light in the UV−visible−NIR region. This wide spectral range is due to the variety of optical transitions that have the potential to be used as DC/UC materials. Hence, trivalent lanthanide ions are proposed as luminescent converters in QDSCs. These lanthanide-doped light-emitting phosphor materials were produced via solid-state/solution/precipitation methods. This paper reviewed the lanthanide ions, their electronic configuration, lanthanide-based light conversion materials, the light conversion mechanism, synthesis methods, and their role in improving the efficiency of QDSCs. Although the concept of using light conversion materials in PVs was laid out about 50 years ago, the improvement of QDSC efficiencies with lanthanide materials is still in its infancy. The development of such kinds of phosphor materials will have a huge impact on enhancing the PCEs of QDSCs. To improve the efficiency of QDSCs, future works should focus on the following, (1) New phosphor materials should be designed with a low phonon energy. (2) New QDs should be designed that have well-matched energy levels with the phosphor materials and also have a wide absorption range of the solar spectrum. (3) Suitable porous materials should be designed for photo-electrodes that adsorb greater numbers of QDs and phosphor-QDs on porous materials through physisorption and chemisorption mechanisms. Charged QDs could be easily adsorbed onto the porous materials through simple electro-static interactions. It has been reported that the number and size of the pores in the metal oxide surfaces are highly significant to adsorb greater numbers of QDs. Further, the functionalization of QDs with molecular linkers is also an approachable way to enhance the adsorption. The linkers chemically attach the QDs to the metal oxide surface and increase the loading of QDs and enhance the charge transfer processes between QDs and metal oxides. (4) Charge recombination should be decreased. (5) The incorporation of plasmonic nanoparticles along with the phosphors is a good idea for future research. Plasmonic nanoparticles have some advantages such as surface plasmon properties, scattering ability, and thermal stability. (6) A separate layer of phosphor materials should be placed either on the top or bottom of the QDSC. In this way, we can achieve a PCE of around 25% in the future.

■ ASSOCIATED CONTENT

Supporting Information

The Supporting Information is available free of charge at https://pubs.acs.org/doi/10.1021/acsomega.2c03736.

Electronic configurations and the radius of lanthanide ions and energy levels of the trivalent lanthanide ions (PDF)

■ AUTHOR INFORMATION

Corresponding Author

Subramania Angaiah − *Electro-Materials Research Laboratory, Centre for Nanoscience and Technology, Pondicherry University, Puducherry 605014, India;* orcid.org/0000-0002-0855-752X; Email: a.subramania@gmail.com

Authors

Ramkumar Sekar − *Electro-Materials Research Laboratory, Centre for Nanoscience and Technology, Pondicherry University, Puducherry 605014, India;* orcid.org/0000-0002-5350-6051

Arrthi Ravitchandiran − *Electro-Materials Research Laboratory, Centre for Nanoscience and Technology, Pondicherry University, Puducherry 605014, India;* orcid.org/0000-0002-8408-6846

Complete contact information is available at: https://pubs.acs.org/10.1021/acsomega.2c03736

https://doi.org/10.1021/acsomega.2c03736
ACS Omega 2022, 7, 35351−35360

Notes

The authors declare no competing financial interest.

■ ACKNOWLEDGMENTS

S.A. gratefully acknowledges the UGC, New Delhi, for financial support under the BSR Mid-Career award scheme (No. F.19-214/2018). R.S. acknowledges the UGC, New Delhi, for providing a Fellowship under the Dr. D.S. Kothari Post-Doctoral Scheme (No.F.4-2/2006 (BSR)/CH/19-20/0143).

■ REFERENCES

(1) Kamat, P. v. Quantum dot solar cells. Semiconductor nanocrystals as light harvesters. *J. Phys. Chem. C* **2008**, *112*, 18737−18753.

(2) Dieke, G. H.; Crosswhite, H. M. The Spectra of the Doubly and Triply Ionized Rare Earths. *Appl. Opt.* **1963**, *2*, 675−686.

(3) Auzel, F. Upconversion and Anti-Stokes Processes with f and d Ions in Solids. *Chem. Rev.* **2004**, *104*, 139−173.

(4) Goldschmidt, J. C.; Fischer, S. Upconversion for photovoltaics - a review of materials, devices and concepts for performance enhancement. *Adv. Opt. Mater.* **2015**, *3*, 510−535.

(5) Dexter, D. L. Possibility of Luminescent Quantum Yields Greater than Unity. *Phys. Rev.* **1957**, *108*, 630−633.

(6) Trupke, T.; Green, M. A.; Würfel, P. Improving solar cell efficiencies by down-conversion of high-energy photons. *J. Appl. Phys.* **2002**, *92*, 1668−1674.

(7) de la Mora, M. B.; Amelines-Sarria, O.; Monroy, B. M.; Hernández-Pérez, C. D.; Lugo, J. E. Materials for downconversion in solar cells: Perspectives and challenges. *Sol. Energy Mater. Sol. Cells* **2017**, *165*, 59−71.

(8) Li, X.; Wang, R.; Zhang, F.; Zhou, L.; Shen, D.; Yao, C.; Zhao, D. Nd^{3+} sensitized up/down converting dual-mode nanomaterials for efficient in-vitro and in-vivo bioimaging excited at 800 nm. *Sci. Rep.* **2013**, *3*, 3536.

(9) Shang, Y.; Hao, S.; Yang, C.; Chen, G. Enhancing solar cell efficiency using photon upconversion materials. *Nanomaterials* **2015**, *5*, 1782−1809.

(10) Wang, F.; Han, Y.; Lim, C. S.; Lu, Y.; Wang, J.; Xu, J.; Chen, H.; Zhang, C.; Hong, M.; Liu, X. Simultaneous Phase and Size Control of Upconversion Nanocrystals through Lanthanide Doping. *Nature* **2010**, *463* (7284), 1061−1065.

(11) Chen, W.; Luo, Q.; Zhang, C.; Shi, J.; Deng, X.; Yue, L.; Wang, Z.; Chen, X.; Huang, S. Effects of Down-Conversion CeO_2:Eu^{3+} Nanophosphors in Perovskite Solar Cells. *J. Mater. Sci.: Mater. Electron.* **2017**, *28* (15), 11346−11357.

(12) Karunakaran, S. K.; Arumugam, G. M.; Yang, W.; Ge, S.; Khan, S. N.; Lin, X.; Yang, G. Research Progress on the Application of Lanthanide-Ion-Doped Phosphor Materials in Perovskite Solar Cells. *ACS Sustain. Chem. Eng.* **2021**, *9* (3), 1035−1060.

(13) Wang, F.; Liu, X. Recent Advances in the Chemistry of Lanthanide-Doped Upconversion Nanocrystals. *Chem. Soc. Rev.* **2009**, *38* (4), 976−989.

(14) Huy, B. T.; Sengthong, B.; van Do, P.; Chung, J. W.; Ajith Kumar, G.; Quang, V. X.; Dao, V. D.; Lee, Y. I. A Bright Yellow Light from a Yb^{3+}, Er^{3+}-Co-Doped Y_2SiO_5 Upconversion Luminescence Material. *RSC Adv.* **2016**, *6* (95), 92454−92462.

(15) Li, C.; Wang, F.; Zhu, J.; Yu, J. C. $NaYF_4$:Yb, Tm/CdS composite as a novel near-infrared-driven photocatalyst. *Appl. Catal., B* **2010**, *100*, 433−439.

(16) Sun, H.; Pan, L.; Piao, X.; Sun, Z. Long afterglow $SrAl_2O_4$:Eu, Dy phosphors for CdS quantum dot-sensitized solar cells with enhanced photovoltaic performance. *J. Mater. Chem. A* **2013**, *1*, 6388−6392.

(17) Sun, H.; Pan, L.; Piao, X.; Sun, Z. Enhanced performance of cadmium selenide quantum dot-sensitized solar cells by incorporating long afterglow europium, dysprosium co-doped strontium aluminate phosphors. *J. Colloid Interface Sci.* **2014**, *416*, 81−85.

(18) Sun, H.; Pan, L.; Zhu, G.; Piao, X.; Zhang, L.; Sun, Z. Long afterglow $Sr_4Al_{14}O_{25}$:Eu, Dy phosphors as both scattering and down converting layer for CdS quantum dot-sensitized solar cells. *Dalton Trans.* **2014**, *43*, 14936−14941.

(19) Wang, K.; Jiang, J.; Wan, S.; Zhai, J. Upconversion enhancement of lanthanide-doped $NaYF_4$ for quantum dot-sensitized solar cells. *Electrochim. Acta* **2015**, *155*, 357−363.

(20) Ramachari, D.; Esparza, D.; López-Luke, T.; Romero, V. H.; Perez-Mayen, L.; de la Rosa, E.; Jayasankar, C. K. Synthesis of co-doped Yb^{3+}-Er^{3+}:ZrO_2 upconversion nanoparticles and their applications in enhanced photovoltaic properties of quantum dot sensitized solar cells. *J. Alloys Compd.* **2017**, *698*, 433−441.

(21) Kaur, R.; Sharma, A. L.; Kim, K. H.; Deep, A. A novel CdTe/Eu-MOF photoanode for application in quantum dot-sensitized solar cell improves power conversion efficiency. *J. Ind. Eng. Chem.* **2017**, *53*, 77−81.

(22) Kubasiewicz, K.; Runowski, M.; Lis, S.; Szczeszak, A. Synthesis, structural and spectroscopic studies on $GdBO_3$:Yb^{3+}/Tb^{3+}@SiO_2 core-shell nanostructures. *J. Rare Earths* **2015**, *33*, 1148−1154.

(23) Fang, D.; Zhang, X.; Zhao, C.; Liu, X.; Shu, X.; Wang, J. Application of bidirectional (up and down)-conversion luminescence material ($GdBO_3$:Yb^{3+}/Tb^{3+}) in $CdSe_{0.4}S_{0.6}$ quantum dot-sensitized solar cells. *Opt Mater.* **2019**, *88*, 80−90.

(24) Khurshid, S.; Latif, H.; Rasheed, S.; Sharif, R.; Sattar, A.; Amjad, R. J. Enhancement in absorption spectrum by ITO coated, down converting glass as a photoanode substrate for efficient PbS/CdS quantum dots sensitized ZnO nano-rods array solar cell. *Opt. Mater.* **2022**, *124*, 111991.

(25) Wang, J.; Wang, F.; Wang, C.; Liu, Z.; Liu, X. Single-Band Upconversion Emission in Lanthanide-Doped $KMnF_3$ Nanocrystals. *Angew. Chem. Int. Ed* **2011**, *123*, 10553−10556.

https://doi.org/10.1021/acsomega.2c03736
ACS Omega 2022, 7, 35351−35360